Japanese Journal of Applied Physics

REGULAR PAPERS

Frequency characteristics of vibration generated by dual acoustic radiation force for estimating viscoelastic properties of biological tissues

Japanese Journal of Applied Physics **57**, 07LF09 (2018)
https://doi.org/10.7567/JJAP.57.07LF09

REGULAR PAPER

Frequency characteristics of vibration generated by dual acoustic radiation force for estimating viscoelastic properties of biological tissues

Ryoichi Watanabe[1*], Mototaka Arakawa[2,1], and Hiroshi Kanai[1,2]

[1]*Graduate School of Engineering, Tohoku University, Sendai 980-8579, Japan*
[2]*Graduate School of Biomedical Engineering, Tohoku University, Sendai 980-8579, Japan*

*E-mail: ryoichi.watanabe@ecei.tohoku.ac.jp

Received November 6, 2017; revised January 1, 2018; accepted January 15, 2018; published online June 5, 2018

We proposed a new method for estimating the viscoelastic property of the local region of a sample. The viscoelastic parameters of the phantoms simulating the biological tissues were quantitatively estimated by analyzing the frequency characteristics of displacement generated by acoustic excitation. The samples were locally strained by irradiating them with the ultrasound simultaneously generated from two point-focusing transducers by applying the sum of two signals with slightly different frequencies of approximately 1 MHz. The surface of a phantom was excited in the frequency range of 20–2,000 Hz, and its displacement was measured. The frequency dependence of the acceleration provided by the acoustic radiation force was also measured. From these results, we determined the frequency characteristics of the transfer function from the stress to the strain and estimated the ratio of the elastic modulus to the viscosity modulus (K/η) by fitting the data to the Maxwell model. Moreover, the elastic modulus K was separately estimated from the measured sound velocity and density of the phantom, and the viscosity modulus η was evaluated by substituting the estimated elastic modulus into the obtained K/η ratio.

1. Introduction

It is well known that the progression of a lesion is accompanied by changes in the hardness and stickiness of the biological tissues, specifically internal living tissues such as muscle, liver, and breast. Therefore, it is important to evaluate the viscoelasticity of the internal living tissues for the rapid detection and quantitative diagnosis of their disorder.[1,2)]

Ultrasound imaging is a noninvasive diagnostic tool highly suitable for viewing living soft tissue.[3–5)] Various methods using ultrasonic imaging have been proposed for characterizing tissues[6–8)] and estimating their displacements.[9–11)] An improvement in image quality has also been reported. In recent years, ultrasonic methods have been studied for the noninvasive evaluation of the elastic properties of living soft tissues. In these methods, the speed of the shear wave or the relationship between the pulse pressure and the change in the diameter of the radial artery was estimated.[12–14)] Methods based on the hysteresis between the applied force and the strain have also been proposed.[15)]

Acoustic radiation force is used for the noninvasive characterization of living tissues. It can generate a displacement inside the living body without damaging the surface. Thus, it is possible to measure the displacement response inside a tissue. Recently, various elastic property measurement methods using acoustic radiation force have been proposed.[16)] Nightingale and coworkers proposed the acoustic radiation force impulse (ARFI) method that applied a pressure to internal tissues using pulsed ultrasonic waves, and evaluated the elastic properties of such tissues from the magnitude of the displacement response.[17–19)] However, a high-intensity pulsed ultrasound of 1,000 W/cm^2 was applied to generate measurable displacement. According to the safety guidelines[20)] for the application of diagnostic ultrasound, it is recommended that the intensity be less than 240 mW/cm^2 for pulse waves and 1 W/cm^2 for continuous waves. Thus, the ultrasonic intensity used by Nightingale and coworkers was markedly beyond the recommended value defined by the safety guidelines. Several other research groups have reported methods using high-intensity pulsed ultrasound to measure the elastic properties of tissues.[21,22)] The use of other methods using a static pressure has also been suggested to estimate the elastic properties.[23)] However, these methods cannot evaluate viscosity because they cannot acquire the frequency characteristics.

To solve these problems, a method of measuring tissue responses to a dynamic pressure was proposed. Fatemi and coworkers excited tissues by using two ultrasound waves with slightly different frequencies. The acoustic radiation pressure applied with the frequency difference of the two ultrasonic waves was generated in the region where two acoustic radiation pressures crossed inside the tissues. The authors experimentally detected hard tissues, such as mineralized tissues, in a soft tissue by measuring the amplitude and phase obtained from the vibration detected by a hydrophone.[24,25)] However, in this method, the direction of the displacement is unknown, and the elastic properties cannot be measured quantitatively.

Another research group has presented the harmonic motion imaging method. This method uses the acoustic radiation force generated by an amplitude-modulated (AM) ultrasonic signal to excite the tissues and measures the displacement response.[26)] The displacement direction, i.e., the excitation direction, is restricted to the irradiation direction because only one transducer is used for the excitation. However, because of a single acoustic radiation pressure, the tissues are forced to move, and the local displacement cannot be generated effectively.

Thus, our group developed a method to locally excite a tissue by applying dual AM acoustic radiation force. The direction of the main displacement to be generated can be fixed to one axis, and it is possible to change the direction of excitation. In previous studies, the fiber structure of muscles as anisotropic samples was excited by dual acoustic radiation force.[27,28)] When the dual transducer was installed parallel to the muscle fiber direction and excited it, local strain was not generated. This showed that local strain was generated by installing dual transducers vertically to the muscle fiber and exciting it. This method can lead to an effective displacement and strain by utilizing the acoustic radiation force.

In another[29)] of our previous studies, the velocity of the shear wave generated by excitation was employed for the

estimation of viscoelasticity. Since an AM ultrasonic wave was used for excitation, it became possible to change the excitation frequency. By scanning the excitation frequency, the generated shear wave at each excitation frequency was observed by the ultrasound diagnostic equipment, and the shear wave velocity was measured for each frequency. By fitting a viscoelastic model to the obtained frequency characteristic of the shear wave velocity, the viscoelasticity of the sample was estimated. Moreover, the visualization of the displacement and propagation of a shear wave in the three-dimensional space inside a tissue was demonstrated.[30] However, since the maximum frame rate of the ultrasound diagnostic equipment employed in these previous studies was 521 Hz, the excitation frequency was restricted to 100 Hz or less.

In the present study, we focused on the fact that the frequency characteristics of the transfer function from stress to strain of the viscoelastic samples depend on the viscoelasticity of the samples. In the present study, therefore, a method of estimating the viscoelasticity of the local region of the samples from the measured frequency characteristics of the local displacement generated by acoustic excitation was proposed. The local region of the phantom simulating the soft tissues was excited at an arbitrary frequency by generating an acoustic radiation force with AM continuous sinusoidal ultrasonic waves irradiated from two directions. The frequency of the applied ultrasound was scanned in the frequency range of 20–2,000 Hz, and the frequency characteristics of the displacement of the phantom were recorded. The viscoelastic parameters were evaluated by fitting the obtained frequency characteristics using the Maxwell model.

2. Experimental methods

2.1 Theory

In the present study, we generated a signal with two frequency components, f_0 and $(f_0 + \Delta f)$, and applied it to two ultrasonic transducers with the same specifications. Thus, we generated two identical acoustic radiation forces. The acoustic radiation force $P_R(d, t)$ applied by a single transducer is given by

$$P_R(d,t) \approx \frac{\alpha p_0^2}{\rho_2 c_2^2} e^{-2\alpha \cdot d}(1 + \cos 2\pi \Delta f t), \quad (1)$$

where α, ρ_2, c_2, p_0, and d are the attenuation coefficient, density, and sound speed of the sample, the sound pressure on the sample surface ($d = 0$), and the distance from the sample surface, respectively.[29] As shown in Fig. 2, the distance d is different from the distance z. The axis along d shows the irradiation direction of ultrasound, and the axis along z shows the direction perpendicular to the sample surface.

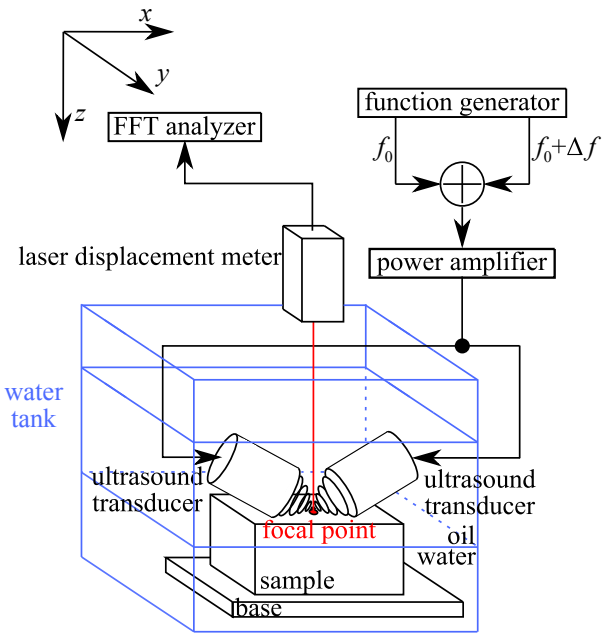

Fig. 1. (Color online) Experimental setup employed in the present study.

If the medium around the target sample is very soft compared with the sample, a single acoustic radiation force can primarily change the position of the sample. Thus, a strain cannot be generated in the local region of the sample, and the mechanical properties of the sample cannot be evaluated. As shown in Fig. 1, in the present study, two transducers are installed obliquely to the surface of the specimen. A force is generated by each transducer in an oblique direction. When the two acoustic forces cross each other, an acoustic pressure of frequency difference Δf is generated in the intersectional region. The forces that synchronize to push the surface of the target sample from both sides are generated using two transducers, and subsequently, a strain can be produced in the sample.

Figure 2 depicts a schematic of the process of straining the sample by bidirectional ultrasonic excitation. On the basis of Eq. (1), the acoustic radiation force acquires the minimum value of 0 when $\cos 2\pi \Delta f t = -1$, as shown in Fig. 2(b). At

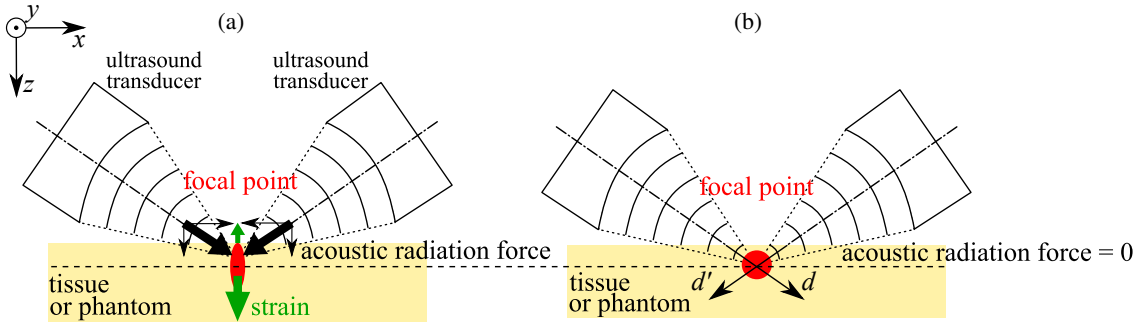

Fig. 2. (Color online) Mechanism of the periodic strain generation by two acoustic radiation forces when (a) $\cos 2\pi \Delta f t = -1$ in Eq. (1) and (b) $\cos 2\pi \Delta f t = 1$ in Eq. (1).

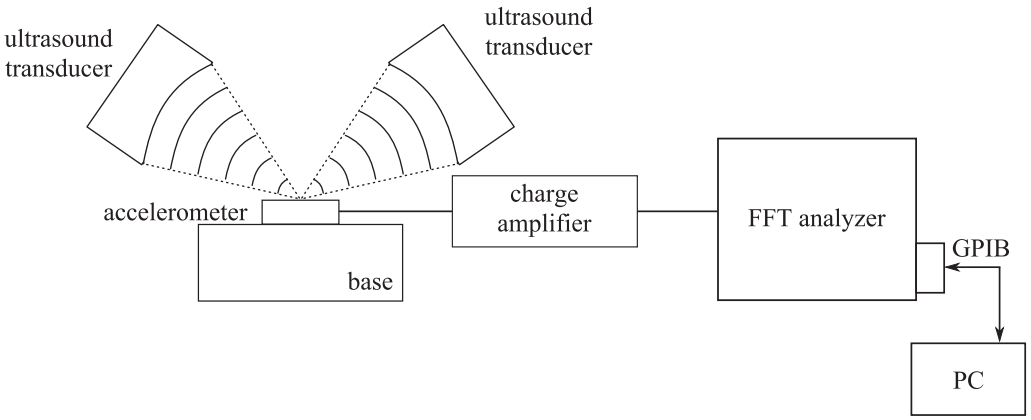

Fig. 3. Experimental setup employed for acceleration measurement.

that time, no force is applied from both sides. In contrast, when $\cos 2\pi\Delta ft = 1$, the acoustic radiation force takes the maximum value of $(2\alpha p_0^2/\rho_2 c_2^2)e^{-2\alpha \cdot d}$, as shown in Fig. 2(a). Thus, the sample is largely strained along the z-axis direction in the focal region. Therefore, a periodic strain of frequency Δf can be locally generated effectively in the vertical direction on the sample surface.[30] At the focal point set inside the sample, the sample is locally strained because it is locally compressed in the horizontal direction and the force is applied in the vertical direction by two acoustic radiation forces.[27]

2.2 Methods

To excite the sample using ultrasonic waves, two continuous sinusoidal waves with frequencies of 1 MHz and 1 MHz + Δf Hz were generated using a function generator (Tektronix AFG2020). The two signals were added together and then amplified using a power amplifier (Yokogawa 7058/10-0). The amplified signal was applied to two point-focusing concave ultrasonic transducers, and the sample was irradiated with ultrasonic waves. In the present study, two transducers with the same specifications namely a center frequency of 1 MHz, an effective aperture width of 50 mm, and a focal length of 60 mm, were installed to intersect their focal points on the sample surface.

In the following experiments, the signal f_0 was fixed to 1 MHz, and Δf was varied from 20 to 2000 Hz. By measuring the displacement generated on the sample surface with a laser displacement meter (Keyence LK-G80) having a resolution of 0.2 μm, we measured the frequency characteristics of the sample displacement caused by the dual acoustic radiation force. We obtained the frequency power spectrum by inputting the measured displacement waveforms to a fast Fourier transform (FFT) analyzer (Ono Sokki CF-940) for each excitation frequency Δf. The power spectra, averaged eight times by the FFT analyzer, were acquired 30 times, from which the average and standard deviations of the power component with Δf were obtained. To eliminate the low-frequency components and electrical noise contaminating the detected displacement signal, frequency analysis was performed to detect only the component of the vibration frequency Δf in the FFT analyzer.

The phantoms mimicking biological soft tissues were prepared by mixing graphite in a ratio of 2% to a urethane resin. Three phantoms with different hardnesses were prepared using gels (Exile H0-100, H5-100, and H15-100) with Asker-C hardnesses of 0, 5, and 15, respectively. In the experiment, an ultrasonic excitation was also applied to granite, a rigid body, for which the viscous component can be ignored. Using the three phantoms with different hardnesses and granite, the differences in the frequency characteristics of the displacement were measured and discussed.

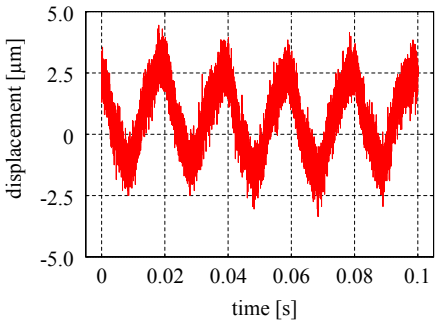

Fig. 4. (Color online) Displacement waveform when the phantom (hardness: 5) was excited at $\Delta f = 50$ Hz.

We also measured the frequency dependence of the acoustic radiation force applied by the ultrasonic transducer. According to the equation of motion $F = ma$, where F is the force, m is the mass, and a is the acceleration, the acceleration is proportional to the force. In the present study, the frequency characteristic of the stress was indirectly evaluated by measuring the frequency characteristic of the acceleration because the stress, which is the force per unit area, and the force are in a linear relationship. For the measurement of the acceleration, a piezoelectric accelerometer (Yamaichi Electronics 111BW) was employed, as shown in Fig. 3. Its resonant frequency was 4 kHz. The acceleration was measured by varying the ultrasonic excitation frequency Δf from 20 to 2,000 Hz. The acceleration signal detected for each Δf was input to the FFT analyzer, and the frequency power spectrum was obtained by averaging 128 power spectra.

3. Results

3.1 Acquisition of frequency characteristic of displacement

The displacement of a phantom was acquired by the laser displacement meter. Figure 4 shows the displacement waveform obtained when the excitation frequency Δf was set to

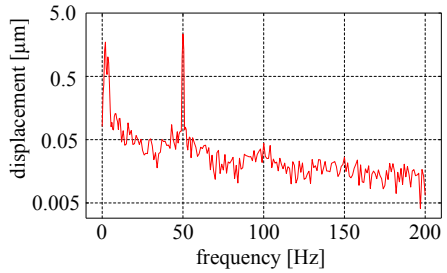

Fig. 5. (Color online) Power spectrum obtained by inputting the displacement waveform in Fig. 4 to the FFT analyzer. The phantom (hardness: 5) was excited at $\Delta f = 50$ Hz.

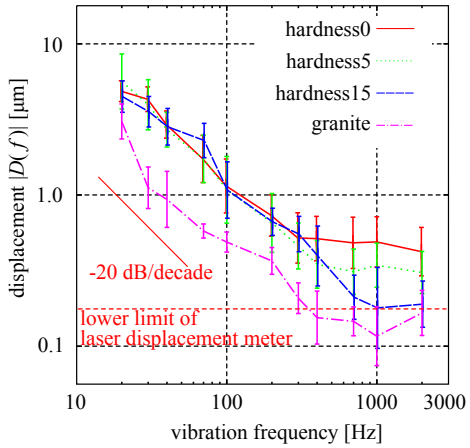

Fig. 6. (Color online) Frequency characteristics of the displacement for the three phantoms with different hardnesses and granite.

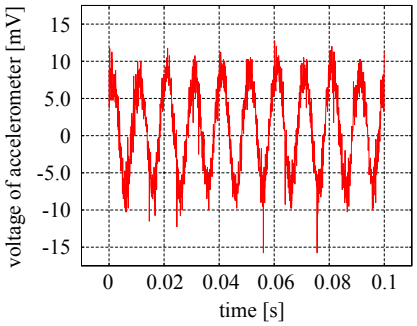

Fig. 7. (Color online) Acceleration waveform when the accelerometer was excited at $\Delta f = 100$ Hz.

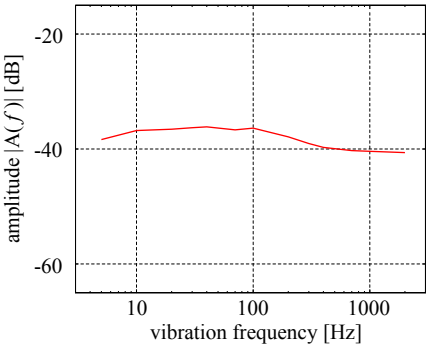

Fig. 8. (Color online) Frequency characteristics of the acceleration amplitude.

50 Hz. The frequency spectrum was acquired by inputting the displacement waveform to the FFT analyzer. Figure 5 displays the average power spectrum when the excitation frequency Δf was set to 50 Hz. By scanning the excitation frequency Δf from 20 to 2,000 Hz, the displacement at each frequency was measured for the three phantoms and granite. The obtained frequency characteristics are shown in Fig. 6.

In each phantom, the displacement decreased with a slope of −20 dB/decade in the frequency range of 20–200 Hz as the vibration frequency increased. In contrast, the displacement became almost constant in the frequency range of 700–2,000 Hz. The frequency at which the displacement became constant increased as the phantom became harder.

For the granite sample prepared as a rigid body, the displacement decreased with a slope of −20 dB/decade in the frequency range of 20–400 Hz. The displacement became almost constant in the frequency range of 400–2,000 Hz. In this frequency range, the displacement was smaller than 0.2 μm, which is the resolution of the laser displacement meter.

3.2 Acquisition of frequency characteristic of stress

The stress at the focal point applied by the dual transducer was acquired by the piezoelectric accelerometer. Figure 7 displays the response of the accelerometer when the excitation frequency Δf was set to 100 Hz. The acquired waveform was a sinusoidal signal.

Figure 8 displays the power spectra of the acquired accelerations shown in Fig. 7 at each excitation frequency Δf. By assuming that the force and acceleration are in a proportional relationship, the frequency characteristic of acceleration $A(\omega)$ in Fig. 8 can be regarded as the frequency characteristic of the ultrasonic excitation stress. From this figure, it can be assumed that there is almost no frequency dependence of the acceleration, that is, practically the same stress was applied to the sample by the acoustic radiation force, regardless of Δf.

3.3 Estimation of viscoelastic properties

The viscoelastic model to be used for fitting was selected. Maxwell and Voight models are typical viscoelastic models. According to the results shown in Fig. 6, the displacement amplitude did not depend on frequency when high-frequency stress was applied. Its behavior follows the Maxwell model. Thus, we fitted the Maxwell model to the experimental results of the frequency characteristics, as shown in Fig. 9. The spectrum magnitude $|H(\omega)|$ in Fig. 9 exhibits the transfer function when the input is the dynamic pressure and the output is the strain, where ω, K, and η are the angular frequency, elastic modulus, and viscosity modulus, respectively. The frequency characteristic of acceleration $|A(\omega)|$ in Fig. 8 is used as the frequency characteristic of the dynamic stress, which corresponds to the input of $H(\omega)$ in Fig. 9(a). The strain is linearly related to the displacement; therefore, the frequency characteristic $|D(\omega)|$ of the displacement in Fig. 6 is the same as the frequency characteristic of the strain corresponding to the output of $H(\omega)$ in Fig. 9(a). Figure 10 shows the frequency characteristics of $|H(\omega)|$ obtained by dividing $|D(\omega)|$ in Fig. 6 with $|A(\omega)|$ in Fig. 8. The characteristic $|H(\omega)|$ in Fig. 10 corresponds to the theoretical graph of the Maxwell model in Fig. 9(b).

By fitting the experimental results of the frequency characteristics in Fig. 10 to the inflection point in the Maxwell model, the K/η ratio between the elastic modulus

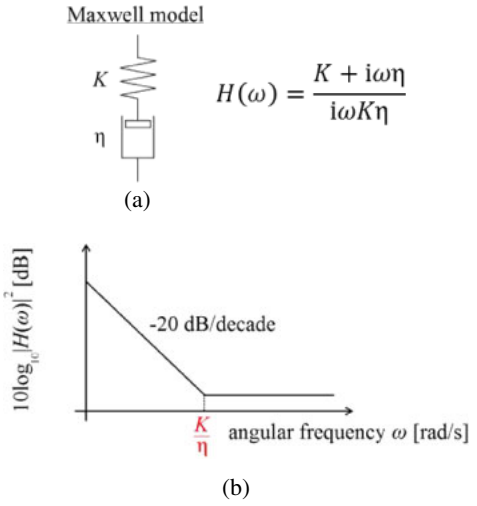

Fig. 9. (Color online) Features of the viscoelastic tissues assuming the Maxwell model. (a) Two elements of the Maxwell model. (b) Frequency characteristics of the strain.

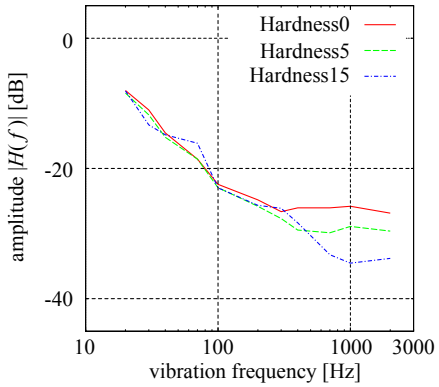

Fig. 10. (Color online) Frequency characteristics of $H(\omega)$ calculated using $D(\omega)$ in Fig. 6 and $A(\omega)$ in Fig. 8.

K and the viscosity modulus η for each phantom was obtained. K/η [s^{-1}] was estimated to be 1.0×10^3, 1.4×10^3, and 2.6×10^3 for the three phantoms with Asker C hardnesses of 0, 5, and 15, respectively. The elastic modulus K increased as the phantoms became harder; therefore, it can be considered that the estimated results of K/η are reasonable. An inflection point also existed in the result of granite as shown in Fig. 6. However, its inflection point would be due to the resolution of the laser displacement meter, not the characteristics of granite, since granite is rigid and its viscosity modulus is very small compared with the elastic modulus. Therefore, the inflection point K/η would exist at a very high frequency for granite. Thus, only the frequency characteristic of granite with a lower frequency than the apparent inflection point was measured in the experiments.

Moreover, we estimated the viscosity modulus η by substituting the elastic modulus K ($=\rho v^2$, ρ: density, v: velocity) into the obtained K/η ratio, where the density ρ was calculated from the ratio of the mass to the volume of the phantom and the sound velocity v was measured by the ultrasonic pulse–echo method. The elastic modulus K was calculated to be 1.95, 2.08, and 2.30 GPa for the three phantoms with Asker C hardnesses of 0, 5, and 15, respectively. By substituting these K values to the obtained K/η ratio, the viscosity modulus η was estimated to be 1.90, 1.48, and 0.89 MPa·s for the three phantoms with Asker C hardnesses of 0, 5, and 15, respectively. The results indicate that the phantom with the hardness of 15 has a higher elastic modulus and the phantom with the hardness of 0 has a higher viscosity modulus. Similar tendencies of the viscoelastic modulus were found in the present and previous studies.[29)]

4. Discussion

4.1 Effect of standing wave

As in these experiments, when pressure was applied to the sample surface, shear waves were generated, and they would be reflected at the edge of the sample surface, producing standing waves. These standing waves could affect the accuracy of the displacement measurement at the focal point. How much they affected the accuracy was confirmed by the following experiments by measuring the behavior of the shear wave propagation.

When acoustic pressures of $\Delta f = 20$, 100, and 500 Hz for one wavelength were applied to the phantom surface, the resultant displacement waveforms were measured at three points on the phantom surface. The phantom with an Asker C hardness of 5 was used as a sample. From the results, the amplitude of reflected waves from the edge of the phantom surface was evaluated.

Figure 11 shows the displacement waveforms measured at three points on the phantom surface when it was irradiated with acoustic radiation pressures of $\Delta f = 20$, 100, and 500 Hz for one wavelength. We measured the displacements at three points of coordinates $(x, y, z) = (0, 0, 0), (0, 6.5, 0), (0, 13.0, 0)$ in Fig. 1 (in mm). The excitation focal point of the phantom surface was at the origin $(0, 0, 0)$, and the edge

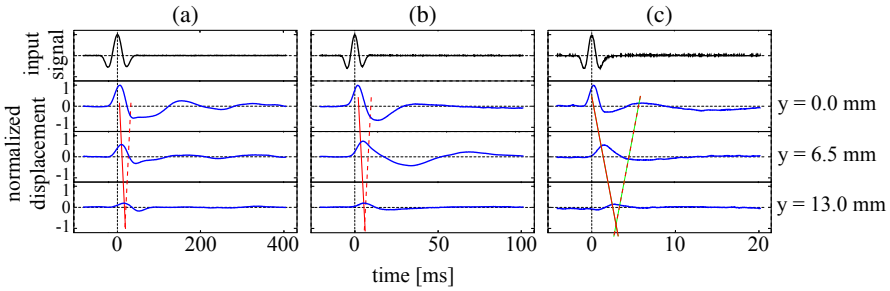

Fig. 11. (Color online) Displacement waveforms at the three points of the phantom (hardness: 5) excited at (a) $\Delta f = 20$ Hz, (b) $\Delta f = 100$ Hz, and (c) $\Delta f = 500$ Hz.

of the phantom was located at $(0, 15.0, 0)$. The red line in Fig. 11 shows how the shear wave propagates, the solid line shows the traveling wave, and the broken line shows the reflected wave. For the vertical axis of Fig. 11, the measured displacement was normalized by the displacement peak value at the focal point.

From these results, the propagation velocities of shear waves generated by 20, 100, 500 Hz excitations were roughly 1.2, 3.8, and 5.5 m/s, and the attenuation coefficients were 1.1, 0.96, and 1.1 dB/mm, respectively. There was 30 mm for this shear wave to reciprocate between the focal point and the edge of the phantom surface. Therefore, when the shear waves returned to the focal point, their amplitudes would be attenuated by −33, −29, and −33 dB, that is, 0.02, 0.03, and 0.02 times the amplitude of the original displacement at the focal point, respectively. The amplitudes of the shear waves which returned to the focal point were much smaller than the standard deviation of the displacements measured in Fig. 6. In the present study, therefore, the standing wave had no fatal effect on the estimation results of the displacements in Fig. 6.

In the displacement waveform at $y = 0$ mm of the phantom excited at 20 Hz, a wave like ringing continued after a positive peak in about 0.15 s. A similar phenomenon was observed for excitation frequencies of 100 and 500 Hz. At any excitation frequency, the phenomenon regarding the wave with a frequency lower than the excitation frequency was observed. In the proposed method, the displacement wave was frequency-analyzed and the power component at the excitation frequency was measured. Therefore, the wave like ringing did not affect the power of the excitation frequency. However, it is still necessary to investigate the cause of this wave in the future.

4.2 Advantages of the proposed method

In the present study, by scanning the excitation frequency more widely than in the previous study, the frequency characteristics of the stress-strain were obtained. From the results, the viscoelastic property of the phantom was estimated. When the Maxwell model was applied, there should only be one inflection point in the frequency characteristics. If there are two inflection points, however, the Zener model using three viscoelastic elements should be applied. Therefore, when the measured frequency range becomes wider and the number of inflection points observed is more than one, a more appropriate viscoelasticity model should be selected.

As a typical method of measuring the viscoelastic property, a rheometer, which sandwiches the sample between two plates and gives dynamic strain, is used to measure the stress generated from the sample by the contacting plate. Thus, it measures the viscoelastic property of the entire sample, which highly depends on the various conditions of the contact between the sample and the plate. In the proposed method, however, by changing the position of the focal point of the acoustic excitation, it is possible to estimate the local region of an internal tissue at each depth separately. Moreover, the spatial resolution of the measurement is higher than that of the rheometer. When measuring the viscoelastic properties of a solid sample with a rheometer, a cylindrical sample with a diameter of about 10 mm or more should be prepared. In the proposed method, on the other hand, the excited region depends on the wavelength of the ultrasonic wave. When an ultrasonic wave of 1 MHz is employed as in the present study, it is possible to excite and estimate a local region of about 2 mm or less. Thus, the proposed method can be applied to lesions of 10 mm or less found in breast, thyroid, and the like.

In the present study, a laser displacement meter was employed for the measurement of the displacement waveform. However, by using ultrasonic diagnostic equipment in the future, the proposed method can be applied to internal tissues that are the main target of measurement in our study. For this purpose, it is necessary to increase the frame rate of the ultrasonic diagnostic equipment. The frame rate can be increased by reducing the depth of field of measurement and increasing the pulse repetition frequency. Therefore, lesions of muscles, breasts and thyroid glands located in a shallow area from the skin are suitable as actual targets of the proposed method. Moreover, by parallel beam forming,[31] which is a technique for increasing the frame rate of the ultrasonic diagnostic equipment, the application of the proposed method to deeply positioned tissues such as liver is anticipated.

5. Conclusions

In the present study, we excited samples by dual acoustic radiation force. We proposed a new method of estimating the viscoelasticity of the excited local region of samples by using the frequency characteristics of the obtained dynamic displacement amplitude. We generated a periodic displacement on the surfaces of phantoms mimicking living soft tissues by irradiating them with the ultrasound generated by the sum of two continuous sinusoidal waves with slightly different frequencies from two directions. The generated displacement was measured using a laser displacement meter. From the frequency characteristics of the displacement and acceleration obtained by varying the excitation frequency Δf, the frequency characteristics of the stress–strain transfer function of the sample were estimated, through which it was confirmed that the ultrasonic excitation stress has almost no frequency dependence. The frequency characteristics of the displacement depended on the hardness of the phantom.

Currently, vibrations at frequencies below 20 Hz are contaminated with large noise in the measurement. If we can accurately measure the frequency characteristics for the lower frequency components, the frequency model will be widely applicable. Furthermore, it is necessary to measure the phase difference between the applied stress waveform and the obtained displacement waveform. If phase information is stably obtained, we can fit the result to a theoretical model such as the Maxwell model in a complex domain including the amplitude and phase. Then, we can select a more appropriate model and improve the fitting accuracy. The establishment of the phase measurement method is one of our future tasks.

1) The Japan Society of Ultrasonics in Medicine, *Shin Cho-onpa Igaku: 1: Iyo Cho-onpa no Kiso* (Igaku Shoin, Tokyo, 2000) p. 115 [in Japanese].
2) S. Chen, M. W. Urban, C. Pislaru, R. Kinnick, Y. Zheng, A. Yao, and J. F. Greenleaf, IEEE Trans. Ultrason. Ferroelectr. Freq. Control **56**, 55 (2009).
3) X. Qu, T. Azuma, H. Imoto, R. Raufy, H. Lin, H. Nakamura, S. Tamano, S. Takagi, S. Umemura, I. Sakuma, and Y. Matsumoto, Jpn. J. Appl. Phys. **54**, 07HF10 (2015).

4) H. Taki, K. Taki, M. Yamakawa, T. Shiina, M. Kudo, and T. Sato, Jpn. J. Appl. Phys. **54**, 07HF05 (2015).
5) Y. Nagai, H. Hasegawa, and H. Kanai, Jpn. J. Appl. Phys. **53**, 07KF19 (2014).
6) H. Isono, S. Hirata, and H. Hachiya, Jpn. J. Appl. Phys. **54**, 07HF15 (2015).
7) T. M. Bui, A. Coron, J. Mamou, E. Saegusa-Beecroft, T. Yamaguchi, E. Yanagihara, J. Machi, S. L. Bridal, and E. J. Feleppa, Jpn. J. Appl. Phys. **53**, 07KF22 (2014).
8) S. Mori, S. Hirata, and H. Hachiya, Jpn. J. Appl. Phys. **53**, 07KF23 (2014).
9) H. Takahashi, H. Hasegawa, and H. Kanai, Jpn. J. Appl. Phys. **54**, 07HF09 (2015).
10) H. Taki, M. Yamakawa, T. Shiina, and T. Sato, Jpn. J. Appl. Phys. **54**, 07HF03 (2015).
11) D. Asari, H. Hasegawa, and H. Kanai, Jpn. J. Appl. Phys. **53**, 07KF21 (2014).
12) Z. Qu and Y. Ono, Jpn. J. Appl. Phys. **54**, 07HF01 (2015).
13) R. Nagaoka, R. Iwasaki, M. Arakawa, K. Kobayashi, S. Yoshizawa, S. Umemura, and Y. Saijo, Jpn. J. Appl. Phys. **54**, 07HF08 (2015).
14) T. Shiina, Jpn. J. Appl. Phys. **53**, 07KA02 (2014).
15) R. K. Parajuli, N. Sunaguchi, R. Tei, T. Iijima, and Y. Yamakoshi, Jpn. J. Appl. Phys. **53**, 07KF30 (2014).
16) J. R. Doherty, G. E. Trahey, K. R. Nightingale, and M. L. Palmeri, IEEE Trans. Ultrason. Ferroelectr. Freq. Control **60**, 685 (2013).
17) K. Nightingale, M. S. Soo, R. Nightingale, and G. Trahey, Ultrasound Med. Biol. **28**, 227 (2002).
18) G. E. Trahey, M. L. Palmeri, R. C. Bentley, and K. R. Nightingale, Ultrasound Med. Biol. **30**, 1163 (2004).
19) B. J. Fahey, K. R. Nightingale, R. C. Nelson, M. L. Palmeri, and G. E. Trahey, Ultrasound Med. Biol. **31**, 1185 (2005).
20) The Japan Society of Ultrasonics in Medicine, Cho-onpa Igaku **11**, 41 (1984) [in Japanese].
21) J. Bercoff, M. Tanter, and M. Fink, IEEE Trans. Ultrason. Ferroelectr. Freq. Control **51**, 396 (2004).
22) K. Masuda, R. Nakamoto, N. Watarai, R. Koda, Y. Taguchi, T. Kozuka, Y. Miyamoto, T. Kakimoto, S. Enosawa, and T. Chiba, Jpn. J. Appl. Phys. **50**, 07HF11 (2011).
23) S. A. McAleavey, M. Menon, and J. Orszulak, Ultrason. Imaging **29**, 87 (2007).
24) M. Fatemi, L. E. Wold, A. Alizod, and J. F. Greenleaf, IEEE Trans. Med. Imaging **21**, 1 (2002).
25) M. Fatemi and J. F. Greenleaf, Proc. Natl. Acad. Sci. U.S.A. **96**, 6603 (1999).
26) K. Michishita, H. Hasegawa, and H. Kanai, Jpn. J. Appl. Phys. **42**, 4608 (2003).
27) H. Hasegawa, M. Takahashi, Y. Nishio, and H. Kanai, Jpn. J. Appl. Phys. **45**, 4706 (2006).
28) Y. Odagiri, H. Hasegawa, and H. Kanai, Jpn. J. Appl. Phys. **47**, 4193 (2008).
29) K. Tachi, H. Hasegawa, and H. Kanai, Jpn. J. Appl. Phys. **53**, 07KF17 (2014).
30) Y. Mochizuki, H. Taki, and H. Kanai, Jpn. J. Appl. Phys. **55**, 07KF13 (2016).
31) H. Hasegawa and H. Kanai, IEEE Trans. Ultrason. Ferroelectr. Freq. Control **55**, 2626 (2008).